Quantifying Model and Image Uncertainty for an OBN dataset in the Norwegian North Sea

Introduction

Seismic velocity models derived via ray-based tomography and full waveform inversion (FWI) are typically non-unique, as the observed data may be explained by many possible models. Constraints may limit these possibilities, but even then many viable models can appear equally correct. Here we present a methodology for quantifying model uncertainty and use the NOAKA ocean bottom node dataset from the Norwegian North Sea to demonstrate our approach.

Method

Our approach builds upon on the work described by Jones et al. (2019), but with some key changes, most importantly in the computation of the prior model covariance for Bayesian uncertainty estimation. In the work of Jones et al. (2019), the prior model is obtained from an intrinsic velocity error which is a function of V_{rms}, the two-way time to a targeted event, and the dominant source frequency. The intrinsic error is hence linked to a variation in velocity that does not produce an observable difference in normal moveout correction under a straight ray approximation due to offset and the frequency band-limit of the data. In this work, we base the prior model uncertainty on three considerations: subsurface structure, global confidence level of the velocity model and an estimate of the illumination given a reference model. We then use ray-based reflection tomography for estimating the posterior uncertainty of the model given prior uncertainties of the model and the data, which for tomography relate to the quality of general moveout curvatures measured from depth-migrated gathers. A Bayesian solution to the tomography problem provides an a posteriori model covariance that is used for perturbing velocity models from a reference model computed from rounds of FWI and tomography. We restrict the perturbations to the velocity model, keeping anisotropy parameters unchanged. The perturbed models, which sample the estimated uncertainty in the model space, are used to map-migrate target horizons to measure the effect of the uncertainty in the migrated image.

The velocity model used here has been derived with Dynamic Matching FWI (DM FWI), which is a robust version of FWI favoring the kinematics given by the acoustic wave equation solution (Huang et al., 2023). The workflow can be summarized as follows:

1. Computation of a reference velocity model estimated from FWI and tomography.
2. Generation of pre-stack depth migrated gathers.
3. Perform generalized moveout picking.
4. Demigration of residual moveout picks to build the tomographic operator.
5. Estimation of the prior model covariance of the reference model.
6. Iterative eigen-decomposition of pre-conditioned tomographic operators to estimate the posterior model covariance.
7. Obtention of N random model realizations from the model posterior - which all fit the tomographic solution within the prior data uncertainty.
8. Re-imaging step on target horizons from the sampled models.
9. Computation of statistical measures.

The posterior model covariance $\mathbf{C_M^{'}}$ to be solved in steps 5 and 6 is given by (e.g., Tarantola, 2004)

$$\mathbf{C_M^{'}} = (\mathbf{A}^T\,\mathbf{C_D^{-1}}\mathrm{A}+\mathbf{C_M^{-1}})^{-1} = \mathbf{C_M}(\mathbf{I}+\mathbf{A}^T\,\mathbf{C_D^{-1}}\mathbf{A}\mathbf{C_M})^{-1} \quad (1)$$

where $\mathbf{A}$ is the tomographic operator given by the demigration of residual moveout picks from a post DM FWI pass of tomography, and $\mathbf{C_D}$ and $\mathbf{C_M}$ are the prior data and model covariances. The data covariance matrix $\mathbf{C_D}$ is a measure of the reliability of residual moveout picks, which in turn is dependent of the SNR of the data after migration. For the a priori model covariance, $\mathbf{C_M}$, this could be established by an overall uncertainty of the prior model from deviations from well data, or from an illumination analysis that takes into consideration data fold and a priori model complexity through ray tracing. The posterior model covariance, $\mathbf{C_M'}$, then measures the uncertainty in the estimated model from residual moveout and the prior data and model uncertainties. Due to the large size of the tomography operator, it is computationally difficult to directly solve for the inverse in Eq. (1). Rather, we apply partial eigen-decomposition to obtain the dominant components for evaluating the posterior uncertainty. In this study, bilateral filtering (Hale, 2011) is used on seismic images to derive a smoothed version of the structure-preserving preconditioner which is then combined with an estimated global confidence level of the current model to generate the prior model covariance. Optionally, The model prior is inversely scaled by a spatially varying illumination field obtained during demigration, For the data prior, a coherence metric tied to each moveout pick is used to address the quality of picked data. A more elegant way of quantifying the data errors is to perform sensitivity analysis of moveout curvatures on the coherence metric and calculate offset dependent vertical deviations from the curvature of the best coherence within some threshold. Using the posterior covariance estimate in Eq. 1, we generate a set of model perturbations from the reference model $\boldsymbol{m}_0$through a set of random vectors $\mathbf{r_i}$:

$$\mathbf{m_i} = \boldsymbol{m}_0 + (diag\ \mathbf{C_M'})^{1/2}\boldsymbol{r_i} \qquad (2)$$

The diagonal elements of the posterior covariance directly measure the uncertainty tied to each model element. The off-diagonal elements represent posterior uncertainty correlation between different parts of the model. A strong correlation between two parameters indicates the model is not independently resolvable (Tarantola, 2005). Here, we constrain our analysis to mapping model uncertainty to the uncertainty of the final migrated volume.

The randomized perturbations in Eq. 2, should not change the overall data misfit since they represent the sampling of the null space in the vicinity of the reference model within the range dictated by the prior data covariance. This can be verified by remigrating with a subset of perturbed models and inspecting the statistical distribution of migration errors. The resultant seismic images will likely have a local shift in response to model perturbations. Via map migrating selected horizons or faults of interest, we can efficiently remap target horizons to establish a statistical evaluation of the uncertainty of the estimated subsurface geology.

Examples

Uncertainty analysis was carried out on a portion of the shallow water (~150 m) NOAKA OBN survey located in the Yggdrasil area of the Norwegian North Sea. Data were acquired over two separate phases in 2021 and 2022 using a triple source configuration, with 25 m shot spacing and 150 m between sail lines. Receiver lines were 300 m apart with a 50 m node spacing within each line.

The geology of the area is typified by a complex overburden, consisting of deltaic fans, channels, injectites, calcite chimneys and other features of highly variable velocity, which need to be accurately modelled in order to correctly image the deeper Cretaceous chalks and highly faulted Jurassic sequences below. These sequences have been identified as areas with exploration potential, so accurate modelling beneath the complex overburden is also required.

The velocity model was derived using a combination of ray-based reflection tomography, incorporating multiple azimuths, and DM FWI using long offset refraction events to capture the background velocity trend & reflection events to model short wavelength complexities in the overburden. Hydrophone data were used for the initial passes of FWI in gradually increasing frequency bands, up to 10 Hz. Subsequent reflection FWI updates, up to a frequency of 15 Hz, were carried out using data after wavefield

separation and Up-Down Deconvolution (UDD) to remove multiple and ghost energy, which helped to stabilise the model update. A data reconstruction methodology was incorporated into the FWI workflow to account for near surface elastic effects, such as guided waves, which were not described by the acoustic modelling. This approach is outlined in greater detail by Zuberi et al. (2023) who show that it preserves the effectiveness of FWI, which otherwise becomes unstable at 6 Hz and above due to the contamination of the hydrophone data with guided waves.

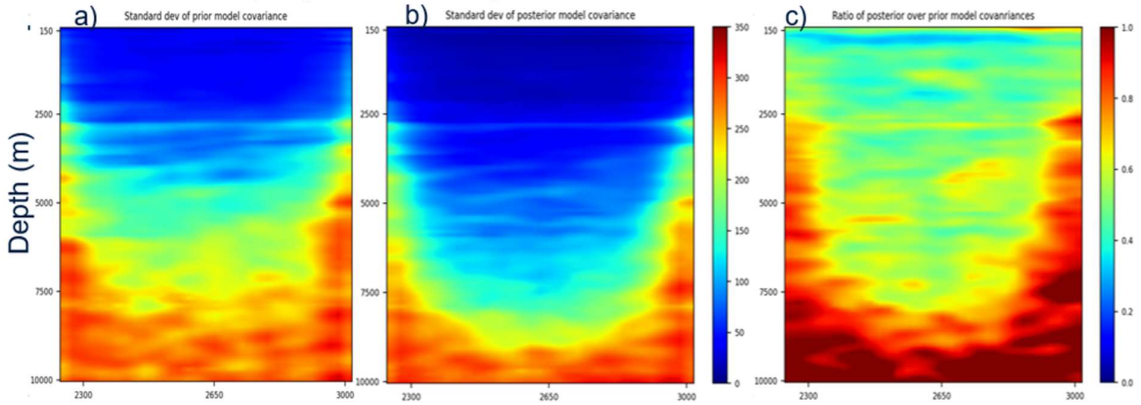

Figure 1 *Standard deviations for prior model covariance (a) and posterior model covariance (b). The ratio of the posteriori and prior model covariances after tomography (c) for a single line.*

In Figure 1, we plot prior and posterior standard deviations from the tomographic uncertainty analysis. The prior standard deviation is constructed from structural information (dip and azimuth of beddings) and prior illumination for the reference model and data geometry. The prior uncertainty does not include information of the SNR in the data, with the uncertainty decreasing with depth due to a decrease in illumination and towards the edges due to lack of fold and aperture. Figure 1b shows the standard deviation after the estimated tomographic uncertainty analysis. Tomography reduces the prior model uncertainty based on the use of residual moveout after migration. The greatest reduction is a function of the angle range of the rays locally, the velocity model, and the quality of the picks used by tomography. The reduction can be quantified by the ratio between these two displays, shown in Figure 1c.

The output from the map migrations is shown in Figure 2a. This example depicts the displacement of a target horizon and a fault produced using 200 randomly perturbed models from equation (2). The uncertainty after tomography predicts a depth displacement of +/- 20 m for the BCU horizon and a lateral displacement of +/- 40 m for the fault in the interval between 3 and 4 km. At larger depths, the displacement predicted by the analysis for the fault plane increases considerably, up to 175 m at 6 km depth, indicating lack of sensitivity to changes in event moveout in this region. The perturbed models produce spatial displacements around the reference models, but do not affect the resolution of the image within the standard deviation of these perturbations. To this end, we gather more statistics by performing depth domain residual move-out correction on the randomly perturbed models and the reference model. We then pick residual moveout on the gathers to produce 200 volumes of *alpha* which measure the deviation from horizontally flattened gathers and interpreted as a ratio of true and migration velocities. A study of these volumes enables us to understand if the model realization randomly drawn from the posterior covariance does not change data misfits in a statistical sense. Figure 2b shows the average difference in the alpha parameter for ten realization models. Each curve in the figure represents one realization model. The vertical axis shows the alpha difference between the realization and the reference gathers, averaged over each line. We can see the difference is limited to 0.002, meaning the velocity difference is roughly smaller than 0.2%. This indicates the randomized model realizations have little impact on the residual moveout statistically, and hence image resolution would not be affected after stacking. Figure 2c shows the alpha difference plotted across all 200 realizations relative to the reference model. Except for two outliers located at the 67th and 120th realizations, the global residual moveout for the realization models are limited to 0.1% relative to the reference model. This

confirms that the randomized model realization from uncertainty analysis essentially samples the null space of the model.

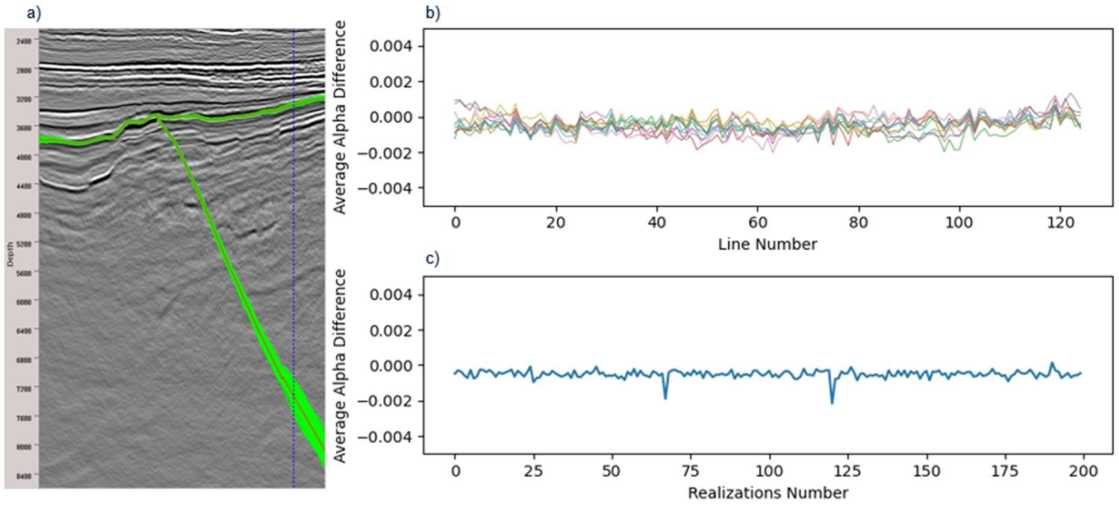

Figure 2. *a) Fault and BCU interpretations with associated uncertainty ranges (green) from map migration with uncertainty realisations; b) Average difference in alpha values as a function of line number for ten realization models. Here each curve represents a single model. c) Alpha differences averaged over all lines across 200 model realizations.*

Conclusions

Recognizing and quantifying uncertainties is pivotal for evaluating risks in interpreting seismic volumes which can then be used in the well planning process. We propose a model building workflow that collates statistics of the derived models and focuses on the key reflections of interest. To reduce computational cost for sampling the model space we rely on ray tracing, although a similar analysis could be performed with a wave equation method. The model statics are used for quantifying how model uncertainty impacts the image used by interpreters in the decision making process. Our approach empowers decision-makers with a low-cost metric set to comprehend and mitigate uncertainties, offering a clearer perspective on the potential risks associated with final seismic interpretations.

Acknowledgements

The authors would like to thank Neil Hurst for interpretation assistance and TGS for permission to present this work.

References

Hale, D., 2011, Structure-oriented bilateral filtering of seismic images, SEG Technical Program Expanded Abstracts : 3596-3600.

Huang, Y., Mao, J., Sheng, J., Perz, M., He, Y., Hao, F., Liu, F., Wang, B., Yong, S., Chaikin, D., Ramirez, A. C., Hart, M., and Roende, H., 2023, Toward high-fidelity imaging: Dynamic matching FWI and its applications, TLE, 124-132.

Jones, I.F., Felicio, R., Vlassopoulou A., 2019 Tutorial: tomographic Bayesian uncertainty estimation. First Break.

Tarantola, A., 2005, Inverse problem theory and methods for model parameter estimation, SIAM, P354.

Zuberi, M. A H., Cho, E., Seher, T., and Myklebust, R., 2023, Mitigating the effects of guided waves in OBN data for acoustic FWI using data reconstruction: A data example from the Yggdrasil area, Extended Abstracts Image Event 2023